Journal of Metals, Materials and Minerals, 34(3), 2038, 2024

High-performance NO_2 gas sensor based on reduced graphene oxide/ZrO_2 hybrids

Ali Jabbar FRAIH[1,*], Nadia NAEEMA[1], and Fatima Fadhil ABBAS[1]

[1] *Department of Physics, College of Science, Wasit University, Iraq*

***Corresponding author e-mail**: alialzubeidy@uowasit.edu.iq

Received date:
24 April 2024
Revised date:
30 May 2024
Accepted date:
24 June 2024

Keywords:
NO_2 gas sensor;
Reduced graphene oxide;
ZrO_2 nanoparticles;
Hybrid materials

Abstract

The increasing concern over environmental pollution, particularly from nitrogen dioxide (NO_2) emissions, necessitates the development of efficient NO_2 detection sensors. This study introduces reduced graphene oxide (rGO)/ZrO_2 hybrids for enhanced NO_2 gas sensing. Utilizing a modified Hummer's method, graphene oxide (GO) flakes were synthesized and subsequently sputtered with 10 nm ZrO_2 film, followed by thermal annealing to produce rGO/ZrO_2 hybrids. The hybrids were characterized using various techniques including SEM, TEM, AFM, Raman spectroscopy, and XRD, confirming successful synthesis and reduction of GO, as well as the formation of ZrO_2 nanoparticles. Gas sensing tests revealed superior sensitivity to NO_2 in the hybrids due to efficient electron transfer between rGO and ZrO_2, resulting in increased hole concentration in rGO and enhanced conductivity. The cyclic performance of the hybrids showed stable response and recovery to NO_2, while selectivity tests demonstrated high sensitivity to NO_2 over other gases including NH_3, ethanol, and oxygen. This study highlights the potential of rGO/ZrO_2 hybrids as high-performance NO_2 gas sensors, offering promising prospects for environmental monitoring and public health protection.

1. Introduction

Rapid population growth drives the need for economic expansion to support livelihoods. However, this growth often leads to environmental challenges, particularly concerning air pollution [1]. Industrial activities are a leading cause of air pollution, particularly in the emission of nitrogen dioxide (NO_2) [2]. This hazardous gas, emitted primarily from vehicular exhausts, power plants, and industrial facilities, poses grave risks to human health and ecosystems, triggering respiratory ailments and exacerbating environmental degradation [3]. Motivated by the urgent need to protect public health and address environmental harm, researchers are increasingly focused on developing better NO_2 detection technologies. Among different techniques, chemiresistors gas sensors have received considerable attention for their simplicity, cost-effectiveness, and scalability [4]. These sensors operate based on changes in electrical resistance upon exposure to target gases [4]. However, selecting the right material for the sensor's channel is crucial for optimal performance.

Even though graphene was discovered in 2004, it remains a highly promising material due to its exceptional properties [5]. This two-dimensional carbon allotrope possesses remarkable physical and chemical properties that make it suitable for a variety of applications, especially for NO_2 gas sensors [3]. Graphene-based chemiresistors offer numerous advantages for NO_2 detection, including reasonable sensitivity, fast response times, and low power consumption [6]. However, when compared to commercial NO_2 sensors, Graphene-based chemiresistors often exhibit lower sensitivity and performance levels. To address these challenges, researchers offer hybrid materials by combining graphene with other nanomaterials. While a variety of nanomaterials are being explored for this purpose, metal oxides stand out as particularly promising candidates due to their high surface area, chemical reactivity, and tunable properties [7]. Up to now, different Graphene/metal oxide structures like Gr/ZnO [8], Gr/SnO_2 [9], Gr/WO_3 [10], Gr/In_2O_3 [11], Gr/NiO [12], and so on are introduced for NO_2 sensing. To the best of our knowledge, no reports have been made on the Zirconium oxide (ZrO_2) nanoparticles for the NO_2 detection. Although individual ZrO_2 nanoparticles are not suitable for this case since it has a very low electrical conductivity, Gr/ZrO_2 hybrids can exhibit promising potentials for enhancing NO_2 sensing capabilities.

In this study, we introduce reduced graphene oxide (rGO)/ZrO_2 hybrids as a novel approach for efficient NO_2 gas sensing. ZrO_2 presents several advantages that make it a promising candidate for NO_2 sensing, including high thermal stability, large surface area, excellent catalytic properties, and chemical inertness [13,14]. These properties can significantly enhance the sensor's performance by providing more active sites for gas adsorption and maintaining structural integrity at high temperatures. Our group is the first to introduce ZrO_2 in combination with reduced graphene oxide (rGO) for NO_2 detection. While our initial findings are promising, further investigations are needed to fully understand and optimize this novel material system. Through a comprehensive synthesis and characterization process involving modified Hummer's method for graphene oxide (GO) synthesis, sputtering of ZrO_2 film, and thermal annealing, we successfully demonstrate the formation of rGO/ZrO_2 hybrids with enhanced NO_2 sensing capabilities. Our investigation reveals efficient electron transfer between rGO and ZrO_2, leading to heightened sensitivity to NO_2, stable cyclic performance, and high selectivity over other gases. This research not only pioneers the development of high-performance NO_2 gas sensors but also offers promising prospects

for their application in environmental monitoring and public health protection.

2. Experimental

2.1 Material

Natural Graphite powder (100 mesh) was acquired from Fluke. Sodium nitrite (99%), sulfuric acid (95% to 98%), potassium permanganate (99%), and hydrochloric acid (37%), hydrogen peroxide (30%) were purchased from Sigma Aldrich. Zirconia - Sputter Target (3 N to 4 N purity) was supplied from Evochem.

2.2 Characterizations

Field emission scanning electron microscopy (Hitachi-S4160) was used to take the morphology of samples. Transmission electron microscopy (CM30m Philips) was utilized to investigate the successful synthesis of GO sheets. Raman spectra were measured by a confocal Raman microscope (Bruker Senterra, 532 nm excitation laser). X-ray diffraction patterns were obtained by PANalytical X'Pert Pro MPD diffractometer. Thickness profiles were taken by atomic force microscopy (AFM) via NOVA NT-MDT SOLVER NEXT, Russia. The NO_2 gas sensing tests were done by a home-made setup including a stainless-steel chamber with connections for electrical measuring, and mass flow controllers which were connected to the Keithley source measure unit (2400, SMU).

2.3 Synthesis of GO sheets

Natural graphite powder (1 g) and sodium nitrate (0.5 g) were mixed in sulfuric acid (20 mL) in an ice-water bath. Then, potassium permanganate (2 g) was gradually added to the mixture and stirred for 60 min. After that, DI water (40 mL) and hydrogen peroxide (200 mL) were added to the mixture, followed by further diluting with hydrochloric acid. The resulting dispersion was centrifuged at 4000 rpm for 2 h and sediments were collected in DI to experience another round of centrifugation. Finally, the remaining sediments were collected in DI and subjected to bath sonication for 2 h resulting in exfoliation of graphite oxide flakes. Then, the dispersion was centrifuged at 2000 rpm for 2 h and the top supernatant was collected as GO sheet dispersion. To prepare the GO film, a few drops of GO dispersion were cast on the quartz substrate and let dry overnight.

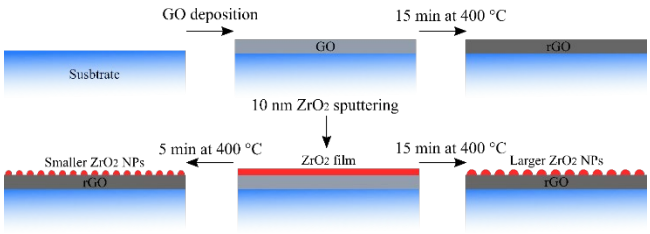

Figure 1. Sensor fabrication process for rGO, 5 min-treated rGO/ZrO_2, and 15 min-treated rGO/ZrO_2 sensors.

2.4 Preparation of rGO/ZrO_2 hybrid

GO/quartz samples were placed in the RF sputtering system and 10 nm ZrO_2 was deposited on them. Then, samples were placed in the quartz tube and annealed at 400°C for 5 min and 15 min under 100 sccm argon flow.

3. Result and discussion

3.1 SEM/TEM characterization of GO sheets

GO sheets are prepared using a modified Hummer's method according to the experimental section [15]. This method is easy and high throughput. Figure 2 (a) shows the morphology of the GO sheets on the substrate. The good concentration of GO flakes allows uniform deposition of them over the substrate. In the context of utilizing GO as the channel of NO_2 sensor, maintaining a good concentration of GO flakes is crucial. An optimal concentration (here 4 $mg \cdot mL^{-1}$) ensures a uniform deposition of GO flakes on the substrate, which is vital for forming a consistent and homogeneous sensing channel. This uniformity is essential for the device's performance, as it enhances the sensitivity and accuracy of NO_2 detection by providing a stable and continuous electrical pathway. Inconsistent deposition could lead to variability in the device's response and compromise the reliability of NO_2 detection. Figure 2(b)) exhibits the higher magnified image of the GO film. Moreover, the TEM image of the GO sheets is shown in Figure 2(c). The layered structure of the GO sheets can be seen in the image. They also show good transparency which refers to efficient exfoliation of the bulk graphite powder.

3.2 Effect of thermal treatment on the formation of rGO/ZrO_2 hybrid

After depositing GO film on the quartz substrate, 10 nm ZrO_2 film was sputtered on them using an RF sputtering system. The thermal treatment is used for two reasons. First, this process promotes the reduction of GO film into the rGO film. Second, thermal treatment helps to convert ZrO_2 films into nanoparticles. In the latter, two annealing times of 5 min and 15 min were investigated to see their effect

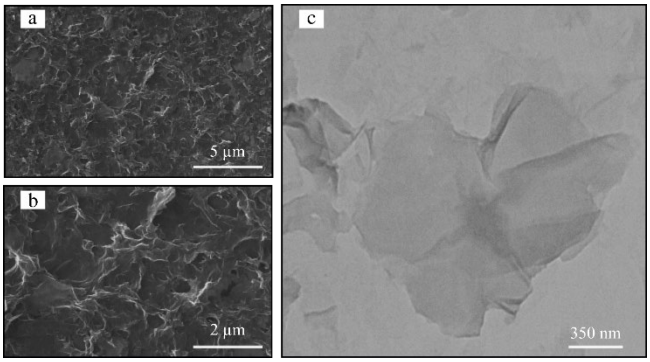

Figure 2. (a) SEM image of the deposited GO film, (b) higher magnification of its surface, and (c) TEM image of the GO sheets.

on the final formation of the hybrids. Figure 3(a-b) shows the SEM image of the hybrid that remained for 5 min at 400°C. The size distribution histogram in Figure 3(c) demonstrates the average size of 39 nm that is distributed in the 20 nm to 60 nm size variation. When samples remained longer (15 min) in the same condition, it was found that it led to a higher average size of 42 nm for the nanoparticle with a wider size distribution (Figure 3(d-f)). This may originate from a combination of more nanoparticles due to their thermal motion during thermal treatment [16].

3.3 Characterization of surface roughness in rGO/ZrO_2 hybrid films via AFM measurements

To see the roughness of the samples, AFM measurements were taken in the non-contact mode. Figure 4(a) exhibits the 3D uniform morphology of GO film with a maximum roughness of 300 nm. In the case of a 5 min thermal treated sample (Figure 4(b)), it has a higher roughness around 500 nm which may be due to the formation of nanoparticles. The AFM image of the 15 min treated sample (Figure 4(c)) demonstrates a higher roughness around 1000 nm that is related to the creation of large nanoparticles in this sample according to the SEM images.

3.4 Electrical conductivity characterization of rGO/ZrO_2 hybrid

To investigate the electrical conductivity of the samples, IV measurements were done by adding silver paste to the samples. Figure 5(a) reveals the IV testing of the samples which is done in the voltage range of -3 V to +3 V and the corresponding currents were measured via the Keithley source measure unit [17]. Accordingly, the GO film shows high resistance with a too-poor electrical current. The 5 min treated sample shows better electrical conductivity and the highest electrical conductivity was measured for the 15 min treated sample. The measured resistance of the samples is shown in Figure 5(b) in which values of 12.1 MΩ, 340 KΩ, and 210 KΩ are calculated for the GO, 5 min, and 15 min treated samples, respectively. The increase of electrical conductivity of two later samples is due to the thermal reduction of GO film into the rGO film [18]. As a result, the 15 min treated film shows higher conductivity since it remains longer time in the 400°C temperature and is subjected to more thermal reductions.

3.5 Raman and XRD characterizations of the thermally formed rGO/ZrO_2 Hhybrid

The thermal reduction of the GO film can also be investigated by Raman spectroscopy. Figure 6(a) shows the Raman spectra of the films. Based on it, the GO film has two Raman peaks around 1351 cm^{-1} and 1600 cm^{-1} that are attributed to D and G phonon oscillations [19]. The same peaks are also observed for the 5 min and 15 min treated films. The ratio of I_D/I_G peak is used to show the degree of GO reduction into the rGO in Figure 6(b) [15]. Based on it, the values of 0.96, 0.86, and 0.83 are calculated for the GO, 5 min, and 15 min treated films, respectively. A reduction in the I_D/I_G ratio is due to the decrease of oxygen-containing functionalized groups in the rGO in comparison with GO sheets [18]. To further investigate this reduction and prove the formation of the ZrO_2 nanoparticles, XRD spectra of the GO and 15 min treated film were provided in Figure 6(c). GO film shows one broad peak around 9.8° that is related to the [001] crystal orientation [20]. In the case of the 15 min treated samples, one strong peak is observed around 24.3° which corresponds to the [002] crystal orientation of the rGO structure and proves its reductions[20]. In addition to this peak, five other peaks appeared around 28.1°, 32.5°, 38.2°, 50.0°, and 58.6° that are related to the [-111], [111], [120], [002], and [131] crystal orientations of the ZrO_2 structure, respectively[21].

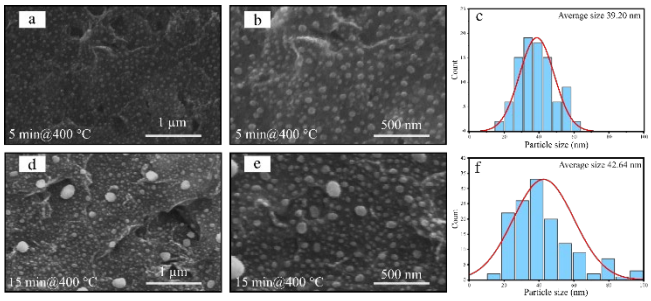

Figure 3. SEM image of hybrids after (a, b) 5 min, and (d-e) 15 min thermal annealing at 400°C. Size distribution histogram of the nanoparticles after (c) 5 min, and (f) 15 min thermal annealing at 400°C.

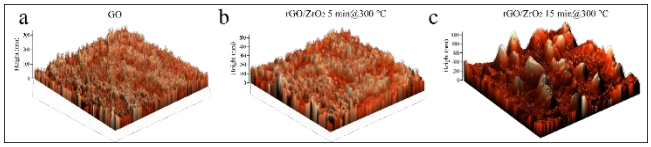

Figure 4. AFM 3d profile of (a) GO, (b) 5 min, and (c) 15 min treated samples at 400°C.

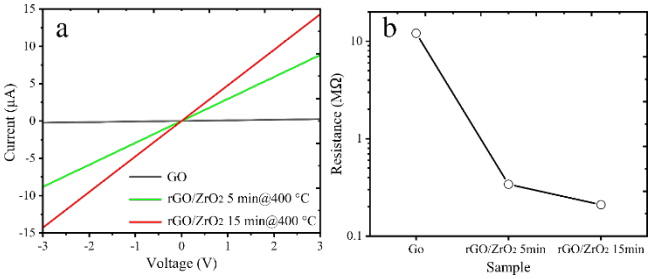

Figure 5. (a) I-V test, and (b) the corresponding resistance of the GO, 5 min, and 15 min treated films.

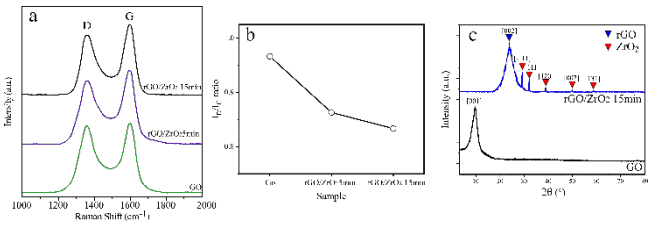

Figure 6. (a) Raman spectra and, (b) corresponding calculated I_D/I_G ratio of the GO, 5 min, and 15 min treated films, and (c) XRD patterns of the GO, and 15 min treated films.

3.6 NO_2 sensing performance of rGO/ZrO_2 hybrid sensors and selectivity analysis

The prepared samples then were used to test NO_2 detection in a home-made setup connected to the SMU system as shown in Figure 7.

The sensitivity is calculated according to the following Equation [3]:

$$S(\%) = \frac{R_{gas}-R_{air}}{R_{air}} \times 100\% \quad (1)$$

Where R_{gas} is the resistance of the sensor upon exposure to NO_2 and R_{air} the resistance of the sensor upon exposure to air. rGO is considered a p-type semiconductor which means its electrical conductivity is dominated by holes [4]. When NO_2 molecules are absorbed on its surface, they extract electrons from the rGO and increase the density of holes in the rGO film [22]. As a result, the overall resistance of the rGO film is decreased upon exposure to the NO_2 gas. The same behavior is observed for the 5 min and 15 min treated rGO/ZrO_2 samples since the rGO is dominant in these samples. According to Figure 8(a), the sensitivity of -24%, -35%, and -28% is measured for the rGO, 5 min, and 15 min treated rGO/ZrO_2 samples under 100 ppm NO_2 concentration, respectively. The rGO/ZrO_2 samples show higher sensitivity compared with the pure rGO due to the electron transfer that happened between them. This electron transfer occurred because the rGO (4.9 eV) [23] has a higher work function than ZrO_2 (3.1 eV) [24], forming a Schottky-type junction between them. Exposure to NO_2 caused electron transfer from ZrO_2 to NO_2, decreasing ZrO_2 carrier concentration [25]. As a result, electrons are transferred back from rGO to ZrO_2, resulting in higher hole concentration in rGO. This led to increased conductivity in rGO, resulting in enhanced sensitivity to NO_2 compared to pure rGO film [25]. Figure 8(b) demonstrates the sensitivity of the samples as a function of different NO_2 concentrations. In rGO, the sensitivity is increased from 6.7% to 24% upon exposure to the NO_2 concentrations from 5 ppm to 100 ppm, respectively. For 5 min treated rGO/ZrO_2, sensitivity shows the value of 15.8% in 5 ppm NO_2 and 35% in 100 ppm NO_2 concentration which are the highest values among two other samples. In the case of 15 min treated rGO/ZrO_2, sensitivity is increased from 9.5% to 28% with increasing the NO_2 concentration from 5 ppm to 100 ppm, respectively. The higher sensitivity of the 5 min treated sample is due to its smaller size nanoparticles that provide a larger surface area and more active sites for absorbing NO_2 molecules [26,27].

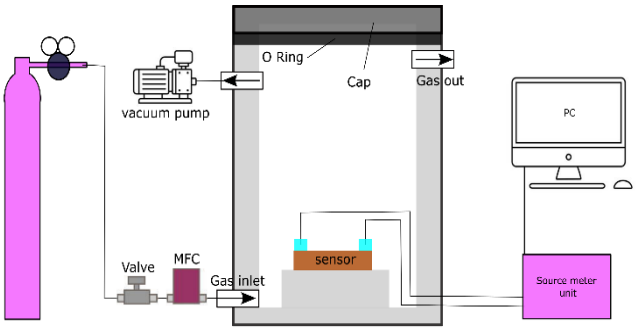

Figure 7. Schematic of the homemade setup for testing the rGO/ZrO_2 sensor.

The cyclic performance of the 5 min treated rGO/ZrO_2 sample is illustrated in Figure 8(c) upon exposure to 100 ppm NO_2 concentration. Based on it, the sample shows a very stable performance both in responding to the gas and recovering to its baseline. Moreover, the selectivity of the sensor was investigated for three other gas species including NH_3, ethanol (C_2H_5OH), and oxygen (O_2). The sensor's responses to NH_3, ethanol, and oxygen alongside NO_2 stem from the rGO's surface interactions with various gas molecules. NO_2, due to its strong oxidizing nature, exhibits the highest sensitivity, whereas NH_3 and ethanol adsorb with lower affinity, causing minor resistance changes. Oxygen interacts by withdrawing electrons, altering rGO conductivity [3,6,11,12,14,22]. According to Figure 8(d), the sensitivity values of -35%, 21%, -4%, and 9% are measured for the 100 ppm concentration of NO_2, NH_3, ethanol, and O_2, respectively. based on it, the highest sensitivity is measured for the NO_2 gas which shows the good performance of the sensor in detecting NO_2 gas. The proposed sensor responds to O_2 as well because oxygen molecules can interact with the rGO surface, altering its electrical properties and thus affecting the sensor's response. Oxygen is a common interfering gas that can influence the conductivity of rGO due to its electron-withdrawing nature, leading to changes in the resistance of the sensor [28]. To address the interference of oxygen in the selectivity of the NO_2 detection, several strategies can be employed. Firstly, surface functionalization of the GO layer with specific groups that have a higher affinity for NO_2 can enhance selectivity [29]. Additionally, incorporating selective coatings or membranes that permit the passage of NO_2 while blocking O_2 molecules can effectively reduce interference [30]. Optimizing the operational temperature and introducing chemical dopants to the GO structure are also viable options to improve selectivity [28].

3.7 Comparative analysis and advantages of rGO/ZrO_2 hybrid sensor for NO_2 detection

The summary of the sensor performance is provided in Table 1 and compared with some sensors reported in other studies. All of them operate at room temperature. Accordingly, the suggested sensor shows very good performance compared with other sensors. In comparison to the WO_3 nanoparticle-loaded MWCNT-rGO hybrids that offer higher sensitivity, the proposed rGO/ZrO_2 hybrid demonstrates distinct advantages, particularly in terms of simplicity, time efficiency, and cost-effectiveness. The rGO/WO_3/MWCNT sensor necessitates a multi-step synthesis process involving the preparation of WO_3 nanoparticles, MWCNT-rGO hybrids, and subsequent sensor fabrication, while our method streamlines the process by directly synthesizing rGO/ZrO_2 hybrids through a straightforward procedure. The synthesis involves the sputtering of ZrO_2 film onto GO/quartz substrates followed by thermal annealing, eliminating the need for complex precursor materials and lengthy synthesis steps. Moreover, the materials used in our synthesis are readily available and cost-effective, further contributing to the overall affordability and accessibility of the sensing platform. Thus, our method presents a promising alternative for efficient NO_2 gas sensing, offering the advantages of simplicity, reduced processing time, and cost-effectiveness, which are essential considerations for scalable sensor fabrication and widespread deployment in real-world applications.

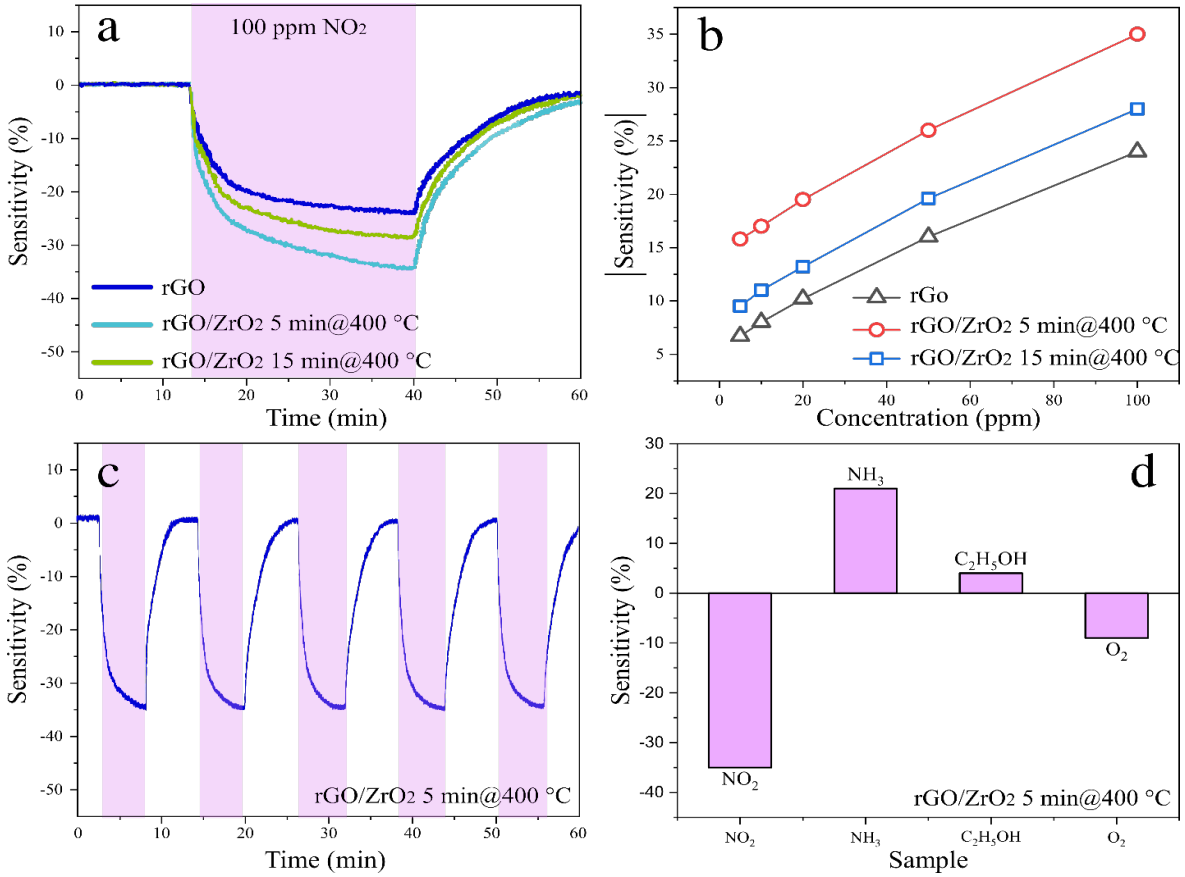

Figure 8. (a) sensitivity of the samples upon exposure to 100 ppm NO_2 gas, (b) sensitivity of the sensors as a function of NO_2 concentrations, (c) cyclic performance of the 5 min treated rGO/ZrO_2 sensors under 100 ppm NO_2 concentration, and (d) selectivity of the 5 min treated rGO/ZrO_2 to NO_2, NH_3, ethanol, and O_2 gas species.

Table 1. The comparison of NO_2 detection performance of rGO/ZrO_2 hybrid with other studies at room temperature testing.

Sensor's material	NO_2 concertation	Sensitivity (%)	Ref.
rGO/ZrO_2	5 ppm	15.8	Present
rGO/ZnO	5 ppm	14.2	[8]
rGO/SnO_2	5 ppm	3.7	[9]
rGO/WO_3/MWCNT	5 ppm	17	[10]
rGO/In_2O_3	30 ppm	8.25	[11]
rGO/NiO/$BiVO_4$	2 ppm	4.3	[12]

4. Conclusions

In conclusion, the study successfully demonstrated the synthesis and characterization of reduced graphene oxide (rGO)/ZrO_2 hybrids for NO_2 gas sensing applications. The hybrids exhibited enhanced sensitivity to NO_2 gas compared to pure rGO, owing to the electron transfer mechanism between rGO and ZrO_2. The thermal annealing process not only facilitated the reduction of GO to rGO but also led to the formation of ZrO_2 nanoparticles, contributing to improved gas sensing properties. The superior sensitivity, stable cyclic performance, and high selectivity of the rGO/ZrO_2 hybrids towards NO_2 highlight their potential for practical applications in environmental monitoring and public health protection. Further optimization of synthesis parameters and exploration of other hybrid materials could lead to even higher-performance gas sensors for various environmental pollutants. This research contributes to the advancement of NO_2 detection technologies and underscores the significance of hybrid materials in enhancing gas sensing capabilities.

References

[1] V. Vyas, K. Mehta, and R. Sharma, "The nexus between toxic-air pollution, health expenditure, and economic growth: An empirical study using ARDL," *International Review of Economics & Finance,* vol. 84, pp. 154-166, 2023.

[2] P. Sicard, E. Agathokleous, S. C. Anenberg, A. De Marco, E. Paoletti, and V. Calatayud, "Trends in urban air pollution over the last two decades: A global perspective," *Science of The Total Environment*, vol. 858, p. 160064, 2023.

[3] F. Ghasemi, "Vertically aligned carbon nanotubes, MoS_2–rGo based optoelectronic hybrids for NO_2 gas sensing," *Scientific Reports*, vol. 10, no. 1, p. 11306, 2020.

[4] A. J. Fraih, and H. M. Mutlaq, "Controlled reduction of graphene oxide via hydrogen plasma for tuning sensitivity and recovery time of rGo based oxygen gas sensor," *European Physical Journal Applied Physics*, vol. 95, no. 3, p. 30101, 2021.

[5] A. J. Fraih, and M. H. J. Alzubaidy, "The effect of graphene layers on the optoelectronic properties of graphene–silicon photodetector," *Journal of Materials Science: Materials in Electronics*, vol. 34, no. 19, p. 1481, 2023.

[6] H. Lim, H. Kwon, H. Kang, J. E. Jang, and H.-J. Kwon, "Semiconducting MOFs on ultraviolet laser-induced graphene with a hierarchical pore architecture for NO_2 monitoring," *Nature Communications*, vol. 14, no. 1, p. 3114, 2023.

[7] W. Eom, J.-S. Jang, S. H. Lee, E. Lee, W. Jeong, I.-D. Kim, S.-J. Choi, and T. H. Han, "Effect of metal/metal oxide catalysts on graphene fiber for improved NO_2 sensing," *Sensors and Actuators B: Chemical*, vol. 344, p. 130231, 2021.

[8] Z. Chen, H. Guo, F. Zhang, X. Li, J. Yu, and X. Chen, "Porous ZnO/rGO nanosheet-based NO_2 gas sensor with high sensitivity and ppb-level detection limit at room temperature," *Advanced Materials Interfaces*, vol. 8, no. 24, p. 2101511, 2021.

[9] H. Bai, H. Guo, C. Feng, J. Wang, B. Liu, Z. Xie, F. Guo, D. Chen, R. Zhang, and Y. Zheng, "A room-temperature chemiresistive NO_2 sensor based on one-step synthesized SnO_2 nanospheres functionalized with Pd nanoparticles and rGO nanosheets," *Applied Surface Science*, vol. 575, p. 151698, 2022.

[10] U. Yaqoob, A. S. M. I. Uddin, and G.-S. Chung, "A high-performance flexible NO_2 sensor based on WO_3 NPs decorated on MWCNTs and RGO hybrids on PI/PET substrates," *Sensors and Actuators B: Chemical*, vol. 224, pp. 738-746, 2016.

[11] F. Gu, R. Nie, D. Han, and Z. Wang, "In_2O_3–graphene nanocomposite based gas sensor for selective detection of NO_2 at room temperature," *Sensors and Actuators B: Chemical*, vol. 219, pp. 94-99, 2015.

[12] S. Bai, K. Zhang, Y. Zhao, Q. Li, R. Luo, D. Li, and A. Chen, "rGO decorated NiO-$BiVO_4$ heterojunction for detection of NO_2 at low temperature," *Sensors and Actuators B: Chemical*, vol. 329, p. 128912, 2021.

[13] G. Feng, Y. Che, S. Wang, S. Wang, J. Hu, J. Xiao, C. Song, and L. Jiang, "Sensitivity enhancement of In_2O_3/ZrO_2 composite based acetone gas sensor: A promising collaborative approach of ZrO_2 as the heterojunction and dopant for in-situ grown octahedron-like particles," *Sensors and Actuators B: Chemical,* vol. 367, p. 132087, 2022.

[14] W. Li, Y. Ren, and Y. Guo, "ZrO_2/ZnO nanocomposite materials for chemiresistive butanol sensors," *Sensors and Actuators B: Chemical*, vol. 308, p. 127658, 2020.

[15] F. Ghasemi, and M. Hassanpour Amiri, "Facile in situ fabrication of rGO/MoS_2 heterostructure decorated with gold nanoparticles with enhanced photoelectrochemical performance," *Applied Surface Science*, vol. 570, p. 151228, 2021.

[16] Y. Altowairqi, A. Alsubaie, K. P. Stroh, I. G. Perez-Marin, L. Bowen, M. Szablewski, and D. P. Halliday, "The effect of annealing conditions: temperature, time, ramping rate and atmosphere on nanocrystal Cu_2ZnSnS_4 (CZTS) thin film solar cell properties," *Materials Today: Proceedings*, vol. 18, pp. 473-486, 2019.

[17] H. M. Mutlaq, and A. J. Fraih, "Controlled plasma tuning of MoS_2 based photodetector: From visible to ultraviolet photo response," *Journal of Metals, Materials and Minerals*, vol. 31, no. 4, pp. 95-101, 2021.

[18] F. Ghasemi, M. Jalali, A. Abdollahi, S. Mohammadi, Z. Sanaee, and S. Mohajerzadeh, "A high performance supercapacitor based on decoration of MoS_2/reduced graphene oxide with NiO nanoparticles," *RSC Advances*, vol. 7, no. 83, pp. 52772-52781, 2017.

[19] B. Zhao, R. Li, Q. Men, Z. Yan, H. Lv, L. Wu, and R. Che, "Transformation of 2D flakes to 3D hollow bowls: Matthew effect enables defects to prevail in electromagnetic wave absorption of hollow rGO bowls," *Small*, vol. 20, no. 3, pp. 2208135, 2024.

[20] S. Rani, M. Kumar, R. Garg, S. Sharma, and D. Kumar, "Amide functionalized graphene oxide thin films for hydrogen sulfide gas sensing applications," *IEEE Sensors Journal*, vol. 16, no. 9, pp. 2929-2934, 2016.

[21] R. Nadhim Shaker, S. Mohammed, and Y. A. Abdulsayed, "Molybdenum disulfide-Zirconium dioxide composite with enhance supercapacitance performance," *Journal of Metals, Materials and Minerals*, vol. 33, no. 4, p. 1791, 2023.

[22] J. -Y. Kang, W. -T. Koo, J. -S. Jang, D. -H. Kim, Y. J. Jeong, R. Kim, J. Ahn, S. -J. Choi, and I. -D. Kim, "2D layer assembly of Pt-ZnO nanoparticles on reduced graphene oxide for flexible NO_2 sensors," *Sensors and Actuators B: Chemical*, vol. 331, p. 129371, 2021.

[23] F. Ghasemi, A. Abdollahi, A. Abnavi, S. Mohajerzadeh, and Y. Abdi, "Ultrahigh sensitive MoS_2/rGo photodetector based on aligned CNT contacts," *IEEE Electron Device Letters*, vol. 39, no. 9, pp. 1465-1468, 2018.

[24] D. Sotiropoulou, and S. Ladas, "The growth of ultrathin films of copper on polycrystalline ZrO_2," *Surface science*, vol. 452, no. 1-3, pp. 58-66, 2000.

[25] Y. Xia, J. Wang, J. -L. Xu, X. Li, D. Xie, L. Xiang, and S. Komarneni, "Confined formation of ultrathin ZnO nanorods/reduced graphene oxide mesoporous nanocomposites for high-performance room-temperature NO_2 sensors," *ACS Applied Materials & Interfaces,* vol. 8, no. 51, pp. 35454-35463, 2016.

[26] J. Hao, D. Zhang, Q. Sun, S. Zheng, J. Sun, and Y. Wang, "Hierarchical SnS_2/SnO_2 nanoheterojunctions with increased active-sites and charge transfer for ultrasensitive NO_2 detection," *Nanoscale*, vol. 10, no. 15, pp. 7210-7217, 2018.

[27] H. Wang, M. Dai, Y. Li, J. Bai, Y. Liu, Y. Li, C. Wang, F. Liu, and G. Lu, "The influence of different ZnO nanostructures on NO_2 sensing performance," *Sensors and Actuators B: Chemical*, vol. 329, p. 129145, 2021.

[28] X. Wang, X. Li, Y. Zhao, Y. Chen, J. Yu, and J. Wang, "The influence of oxygen functional groups on gas-sensing properties of reduced graphene oxide (rGO) at room temperature," *RSC Advances*, vol. 6, no. 57, pp. 52339-52346, 2016.

[29] Y. R. Choi, Y. -G. Yoon, K. S. Choi, J. H. Kang, Y. -S. Shim, Y. H. Kim, H. J. Chang, J. -H. Lee, C. R. Park, S. Y. Kim, and H. W. Jang, "Role of oxygen functional groups in graphene oxide for reversible room-temperature NO_2 sensing," *Carbon*, vol. 91, pp. 178-187, 2015.

[30] T. Han, S. Gao, Z. Wang, T. Fei, S. Liu, and T. Zhang, "Investigation of the effect of oxygen-containing groups on reduced graphene oxide-based room-temperature NO_2 sensor," *Journal of Alloys and Compounds*, vol. 801, pp. 142-150, 2019.